Journal of Advanced Ceramics
2019, **8**(2): 218–227
https://doi.org/10.1007/s40145-018-0307-z
ISSN 2226-4108
CN 10-1154/TQ

Research Article

Mechanical properties and thermal stability of carbon fiber cloth reinforced sol-derived mullite composites

Wei ZHANG[a,b], Qingsong MA[b,*], Kuanhong ZENG[b], Songlin LIANG[b], Weiguo MAO[a,*]

[a]*School of Materials Science and Engineering, Xiangtan University, Xiangtan 411105, Hunan, China*
[b]*Science and Technology on Advanced Ceramic Fibers & Composites Laboratory, National University of Defense Technology, Changsha 410073, China*

Received: August 30, 2018; Revised: November 5, 2018; Accepted: November 21, 2018

Abstract: For the wide application as thermal protection materials, it is very necessary for mullite ceramics to improve fracture toughness. In this paper, the laminated and stitched carbon fiber cloth preform reinforced mullite (C/mullite) composites were prepared through the route of sol impregnation and heat treatment using the Al_2O_3–SiO_2 sol with a high solid content as raw materials. The C/mullite composites showed a flexural strength of 228.9 MPa that was comparable to that of dense monolithic mullite although the total porosity reached 13.4%. Especially, a fracture toughness of 11.2 MPa·m$^{1/2}$ that was 4–5 times that of dense monolithic mullite was obtained. Strength deterioration due to the carbothermal reduction between carbon fiber and the residual SiO_2 in matrix was found above 1200 ℃. A pyrolytic C (PyC) coating was deposited on carbon fibers as interfacial coating. The chemical damage to carbon fibers was obviously alleviated by the sacrifice of PyC coating. Accordingly, the C/PyC/mullite composites kept strength unchanged up to 1500 ℃, and showed much higher strength retention ratio than C/mullite composites after annealing at 1600 ℃.

Keywords: carbon fiber reinforced mullite composite; sol; mechanical property; thermal stability

1 Introduction

In despite of some advantages such as low density, low thermal expansion, desirable thermal stability, and oxidation resistance [1–6], the inherent brittle fracture behavior limits the structural applications of mullite ceramics. Incorporating the second phases can improve the fracture toughness of monolithic mullite. Of all the second phases, continuous fiber reinforcement is superior due to the outstanding damage tolerance. Furthermore, three-dimensional (3D) fiber preforms, for example, 3D braided fiber, laminated and stitched fiber cloth, and 3D fiber needled felt, have been extensively employed as the reinforcement for high performance composites owing to its better flexibility in structure design, desirable comprehensive performance, and good adaptability to complex shape. So far, oxide fibers have been extensively employed to reinforce mullite [7–13], whereas carbon fiber was scarcely used, not to mention 3D carbon fiber preform. Wu *et al*. [14,15] once fabricated unidirectional carbon fiber reinforced mullite composites by filament winding, stacking, and hot-pressing. Although the resulting composites showed

* Corresponding authors.
E-mail: Q. Ma, nudtmqs1975@163.com; W. Mao, ssamao@126.com

high mechanical properties in *X* direction, the interlaminar strength and the in-plane strength were low due to the absence of carbon fiber in *Y* and *Z* directions. Furthermore, this route is difficult for the fabrication of large-size components with complex shape.

Taking the structural characteristics of 3D fiber preform and the fabrication of large-size complex components into account, the gas infiltration and the solution impregnation routes are preferable for the sake of homogeneous distribution of matrix and low fabrication temperature. However, there is no proper gaseous raw material for the co-deposition of Al_2O_3–SiO_2 at present. The transformation efficiency from solution via sol-gel to Al_2O_3–SiO_2 is very low, resulting in 3D fiber reinforced mullite composites with high porosity and low strength [16]. Recently, the fabrication of 3D oxide and SiC fiber preforms reinforced oxide ceramic composites from sols with high solid content has drawn increasing interests [7–9,17,18]. The route of sol impregnation–drying–heat (SIDH) treatment is promising since it improves the fabrication efficiency of solution impregnation route and reserves the advantages of homogeneous distribution of matrix and low fabrication temperature.

Using 3D carbon fiber preform as reinforcement, the authors have fabricated 3D C/Al_2O_3 [19] and C/YAG (yttrium aluminum garnet, $Y_3Al_5O_{12}$) [20,21] composites through the SIDH route. The former studies indicated that the characteristics of sol and the structure of fiber preform had great influence on the processing and mechanical properties of 3D fiber composites. Depending on the compositions of Al_2O_3 sol and Y_2O_3–Al_2O_3 sol, the Al_2O_3 and Y_2O_3–Al_2O_3 gel powders exhibited different sintering shrinkage behaviors. Although the ceramic yield and viscosity of the two sols were almost the same, the fabrication of C/Al_2O_3 and C/YAG composites with the same reinforcement needed different sintering schedule and SIDH cycles, and the as-received composites had different total porosity and mechanical properties [19,20]. For C/YAG composites, even if the sol and the processing were the same, different carbon fiber preforms resulted in different microstructure and mechanical properties because of the different fiber distribution and pore structure [20,21]. Therefore, the processing should not be copied for different C/oxide composites.

In addition, 3D C/mullite composites were also prepared through the SIDH route in our previous work [22–25]. 3D braided carbon fiber preform and three kinds of SiO_2-rich Al_2O_3–SiO_2 monophasic sols were used as reinforcement and raw materials for mullite matrix, respectively. The resultant 3D C/mullite composites had high total porosity of which ~50% was close porosity because of the viscous flow of rich SiO_2 as well as the preform structure. In order to reduce the porosity, the diphasic Al_2O_3–SiO_2 sol with stoichiometric ratio of mullite ($3Al_2O_3{\cdot}2SiO_2$) was used as the precursor for mullite matrix in this paper. With regards to the reinforcement, the laminated and stitched fiber cloth preform was selected because its structure is open and easy for sol to impregnation. Moreover, the laminated and stitched fiber cloth preform has high performance-to-cost ratio among the 3D fiber preforms because it integrates the high performance of 3D braided fiber with the low cost of 3D fiber needled felt.

As mentioned above, since both the sol and the reinforcement were changed, it is necessary to restudy the processing and mechanical properties of C/mullite composites. Thus, the mullitization and sintering shrinkage of the diphasic Al_2O_3–SiO_2 sol with stoichiometric ratio of mullite ($3Al_2O_3{\cdot}2SiO_2$) were firstly studied to decide the fabrication temperature of 3D C/mullite composites. Then the mechanical properties and thermal stability of 3D C/mullite composites were investigated in this study.

2 Experimental

Al_2O_3 sol and SiO_2 sol were blended according to the stoichiometric mullite ($3Al_2O_3{\cdot}2SiO_2$). The resultant Al_2O_3–SiO_2 sol with a solid content of 30.7 wt% and a viscosity of 8.8 mPa·s was used as precursor for mullite matrix. Gel powders were obtained after the sol was dried at 200 ℃. The gel powders were heated at various temperatures under inert atmosphere, followed by phase composition analysis through X-ray diffraction (XRD). XRD was carried out on a diffractometer (Bruker D8 advance) with Cu Kα radiation. Data were digitally recorded during a continuous scan in the range of angle (2θ) from 10°–80° with a scanning rate of 4 (°)/min. In addition, the gel powders were cold pressed to wafers at 120 MPa. Linear shrinkage of the wafers after heat treatment was measured.

Plain weave carbon fiber cloths were laminated and stitched with carbon fiber bundles to form the 3D carbon fiber preform (T300 3k, ex-PAN carbon fiber, Toray) with a fiber volume fraction of 45%. The density of carbon fiber was 1.76 g/cm^3. The 3D carbon

fiber preform was desized by thermal treatment at 1400 ℃ for 1 h [26,27], followed by vacuum impregnation of sol. After soaked in sol for 6 h, the preform was dried at 200 ℃ for 2 h and then heated at 1300 ℃ for 1 h under inert atmosphere with a heating rate of 15 ℃/min. The fabrication of C/mullite composites was completed after the cycle of impregnation–drying–heating repeated 28 times. In order to study the effect of interfacial coating on mechanical properties and thermal stability, the composites with PyC interfacial coating were also fabricated through the same processing. The PyC coating was prepared on fiber surface after desizing by CVD with CH_3CHCH_2 as raw materials. The as-received C/mullite composites were annealed at different temperatures under inert atmosphere for 1 h to characterize thermal stability.

The apparent density (ρ_a) of C/mullite composites was computed from the weight-to-volume ratio. The bulk density and open porosity were measured according to the Archimede's principle with deionized water as immersion medium. The theoretic density (ρ_T) of C/mullite composites was calculated from Eq. (1):

$$\rho_T = V_f \times \rho_f + V_m \times \rho_m \quad (1)$$

where V_f (45%) and V_m (55%) are the volume fractions of fiber and matrix, ρ_f (1.76 g/cm^3) and ρ_m (3.17 g/cm^3 [1]) are the densities of fiber and matrix, respectively. Thus, total porosity was equal to $1-\rho_a/\rho_T$ and the open porosity subtracted from total porosity gives close porosity.

Three-point bending test was employed to evaluate the flexural strength and elastic modulus of C/mullite composites with a span/height ratio of 15 and a cross-head speed of 0.5 mm/min. The fracture toughness was determined by the single edge notched beam (SENB) method with a cross-head speed of 0.05 mm/min and a span/height ratio of 4. The ratio of notch depth to specimen height was 0.50. Five specimens were tested to obtain the average strength and fracture toughness. Fracture work was calculated from the formula of $W = A_C/BH$ [28], where A_C was the characteristic area of fracture curve, which refers to the area under load–displacement curve above 90% stress; H and B are the thickness and width of the sample, respectively. Weight loss and flexural strength retention after annealing were recorded to characterize thermal stability of C/mullite composites. Scanning electron microscopy (SEM) and energy dispersive spectroscopy (EDS) (Quanta-200 EDAX) were employed to observe microstructures and measure element compositions of the composites.

3 Results and discussion

3.1 Fabrication and mechanical behavior of C/mullite composites

The phase compositions of gel powders after heat treatment are shown in Fig. 1. The original gel powder is amorphous. Only metastable Al_2O_3 phases were observed during 1000–1200 ℃. The metastable Al_2O_3 phases were underdeveloped because of the faint peak intensity. The absence of SiO_2 diffraction peak indicated the amorphous state of SiO_2. At 1300 ℃, all diffraction peaks can be assigned to mullite phase. Moreover, the peak intensity is high. These suggested that the mullitization was basically completed, which was decided by the high reactivity of underdeveloped metastable Al_2O_3 phase and amorphous SiO_2. With increasing temperature to 1400 ℃, peak intensity is further strengthened, indicating the enhanced crystallinity of mullite.

By comparison, it can be found that the characteristics of sol determined the mullitization behavior. The Al_2O_3–SiO_2 sols with different Al_2O_3/SiO_2 mass ratio in previous studies [23–25] were synthesized from the co-hydrolysis of Al- and Si-containing alkoxides or inorganic salts. They were called monophasic sol since Al–O–Si bond was formed in sol. The mullitization of this sol took place at temperature as low as 900–1000 ℃ due to the homogeneity at atomic level [29]. So, mullite peak at ~26° was observed at 1000 ℃ and mullitization occurred to a great extent at 1200 ℃ [23–25]. On the contrary, for diphasic sol in this paper, the mullite was formed at 1300 ℃ because the homogeneity scale was between 1 and 100 nm [29]. In

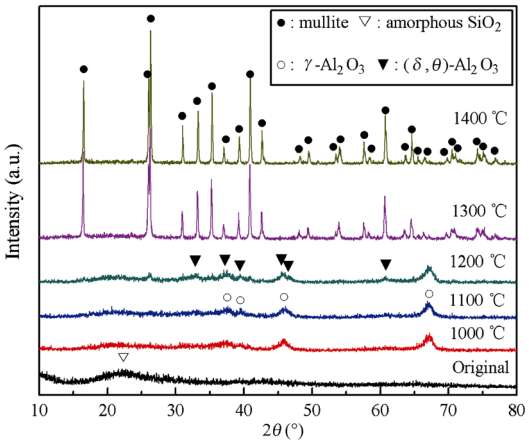

Fig. 1 XRD patterns of gel powders after heat treatment at different temperatures.

addition, the transformation of metastable Al_2O_3 phases before mullitization was not observed for monophasic sol [23–25].

Figure 2 shows the relation between heat treatment temperature and linear shrinkage of gel powder wafers. As shown, the linear shrinkage increased from 13.6% at 1000 ℃ to 22.9% at 1300 ℃, approximately corresponding to the direct proportion law. The obvious shrinkage is beneficial to the densification of matrix and can be ascribed to the viscous flow of SiO_2. The SiO_2 was consumed to create mullite at 1300 ℃, impairing the viscous flow of SiO_2. Accordingly, a little increment (0.6%) in linear shrinkage was detected from 1300 to 1400 ℃. For monophasic sol, the linear shrinkage was almost unchanged during 1200–1400 ℃ due to the obvious formation of mullite at 1200 ℃ [24].

Based on the XRD and linear shrinkage results, the heat treatment during the fabrication of C/mullite composites was conducted at 1300 ℃. The C/mullite composites without interfacial coating showed an apparent density of 2.19 g/cm^3 and an open porosity of 11.3%. The theoretical density was computed as 2.53 g/cm^3. Thus, the total porosity was 13.4% and the close porosity was 2.1%. By comparison, the composites derived from SiO_2-rich sol showed much higher total porosity (21%–26%) and close porosity (11%–14%) [23–25]. The structure of fiber preforms and the characteristics of sols were responsible for the different porosity. On one hand, as compared with 3D braided carbon fiber preform, the laminated and stitched fiber cloth preform was deficient in the connection between the two adjacent layers. This more open structure was advantageous to the diffusion of sol, and then reduced the total porosity. On the other hand, the Al_2O_3–SiO_2 sol in this study was not rich in SiO_2. Thus, the formation of close pores due to the viscous flow of rich SiO_2 was effectively suppressed.

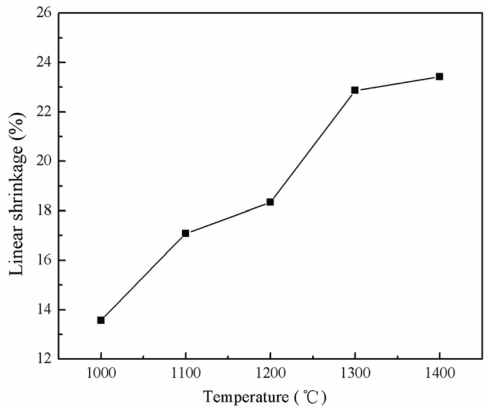

Fig. 2 Linear shrinkage of gel powder wafers after heat treatment.

The flexural strength and the fracture toughness of the C/mullite composites without interfacial coating were 228.9 MPa and 11.2 MPa·m$^{1/2}$, respectively. The flexural strength is comparable to that (200–300 MPa) of monolithic mullite ceramics, and the fracture toughness is 4–5 times that of monolithic mullite ceramics [1]. The fracture work was calculated as 6120 J/m^2, which is over tenfold higher than that of monolithic ceramics. Profiting from the lower porosity, the mechanical properties in this study were almost equal to those of the 3D braided C/mullite composites even if the fiber fraction in *X* direction (~22.5%) was lower than that of the 3D braided fiber preform (~38.3%) [24].

The stress–strain curve and the fracture surface of the C/mullite composites without interfacial coating are presented in Figs. 3 and 4, respectively. A maximum strain of ~0.9% at invalidation point and the circuitous decline of load after this point were observed in Fig. 3. Figure 4 shows extensive fiber pull-out and long pull-out length. The fiber pull-out can dissipate crack-tip energy

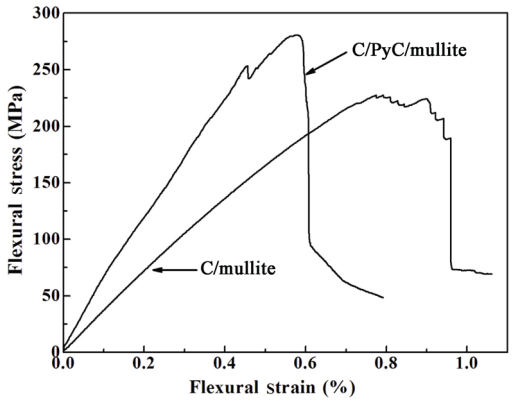

Fig. 3 Stress–strain curves of the C/mullite and the C/PyC/mullite composites.

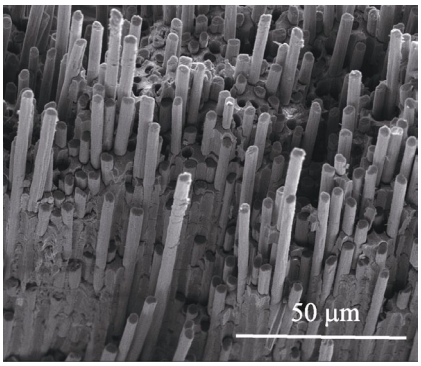

Fig. 4 SEM photo of fracture surface of the C/mullite composites without interfacial coating.

and make crack deflect, leading to the non-catastrophic fracture behavior shown in Fig. 3. The prominent toughening effect of continuous fiber reinforcement was demonstrated.

In addition, the tough fracture behavior indicated that the interfacial bonding between carbon fiber and mullite was mainly physical bonding. Continuous fiber reinforced ceramic matrix composites are fabricated at high temperature along with high pressure sometimes. Once the chemical bonding was created, the fiber strength must be seriously deteriorated and the interfacial bonding is certain to be strong, resulting in flat fracture surface with little fiber pull-out and low fracture toughness. On the other hand, in the similar study of Wu *et al*. [30], no obvious chemical reaction between carbon fiber and mullite matrix during the hot-pressing at 1300 ℃ was found through transmission electron microscopy (TEM) observations.

3. 2 Thermal stability of C/mullite composites

Table 1 presents the weight loss and the flexural strength retention ratio of the C/mullite composites after annealing. The elemental analysis of the matrix close to fiber after annealing is listed in Table 2. The data in Table 1 indicated that the C/mullite composites without interfacial coating could retain its flexural strength up to 1200 ℃.

Although the EDS result is semi-quantitative, the variation trend can provide the evolution information of matrix composition. It is found from Table 2 that there was a slight decline in the contents of Si and O after annealing at 1200 ℃. This might be caused by carbothermal reduction due to the high reactivity between the disorder carbon on fiber surface [26,27] and a small quantity of unreacted amorphous SiO_2.

Table 1 Weight loss and mechanical properties of C/mullite composites after annealing

Annealing temperature (℃)	1200	1400	1600
Weight loss (%)	0.64	0.83	17.20
Strength retention ratio (%)	103.10	84.60	29.30
Fracture work retention ratio (%)	105.20	92.30	19.60

Table 2 Elemental analysis results of the matrix close to fiber in C/mullite composites

Annealing temperature (℃)	As-received	1200	1400	1600
C (at%)	31.32	41.08	45.05	71.16
O (at%)	38.78	37.26	34.64	13.73
Al (at%)	23.32	15.66	15.81	12.55
Si (at%)	6.58	6.00	4.49	2.56

Based on the thermodynamic data, the reactions of $C+Al_2O_3$ and $C+3Al_2O_3{\cdot}2SiO_2$ do not occur before 1810 ℃. Therefore, the two reactions are impossible in this study since the maximum annealing temperature was 1600 ℃. The only possible chemical reaction is the carbothermal reduction between C and SiO_2. The SiO_2 was derived from the unreacted SiO_2 during mullitization and the decomposition of mullite above 1550 ℃.

For diphasic gel, the activation energy for mullite crystallization was much higher than that of monophasic gel and the mullitization was controlled by the diffusion of Si and Al in the created mullite interface [29]. It has been found that the complete densification of diphasic gel at 1250−1500 ℃ was due to the residual SiO_2 and the residual SiO_2 usually remained in the final product [29,31]. Tkalcec *et al*. [32] revealed that the mullite fraction was ~70 wt% when the diphasic gel was heated at 1300 ℃ for 6 h. Thus, it is sure that there was a small quantity of unreacted amorphous SiO_2 after the fabrication of C/mullite composites at 1300 ℃. According to the study of Vix-Guterl and Ehrburger [33], the lowest temperature of carbothermal reduction was 1220 ℃. Therefore, the carbothermal reduction between the disorder carbon on fiber surface and the unreacted amorphous SiO_2 was very likely to happen at 1200 ℃. Of course, this reaction was faint at 1200 ℃ and the resultant chemical damage to fiber was not obvious. Accordingly, the composites kept its flexural strength and fracture work unchanged. At 1400 ℃, the carbothermal reduction began to be active, and the obvious decrease in the contents of Si and O was detected. This brought on a higher weight loss. However, the flexural strength and fracture work decreased a little, suggesting that the chemical damage to carbon fiber was not high.

It has been reported that the mullite would dissociate into Al_2O_3 and SiO_2 above 1550 ℃ [34]. This was also verified in this study. The XRD pattern of Al_2O_3–SiO_2 gel after heat treatment at 1600 ℃ is shown in Fig. 5. The obvious peaks of α-Al_2O_3 demonstrated the decomposition of mullite at 1600 ℃. The created SiO_2 was amorphous or had low crystallinity since no peak of crystalline silica was observed in Fig. 5. At 1600 ℃, the created SiO_2 was consumed by carbon fiber through carbothermal reduction. As a result, the contents of Si and O elements were reduced by about

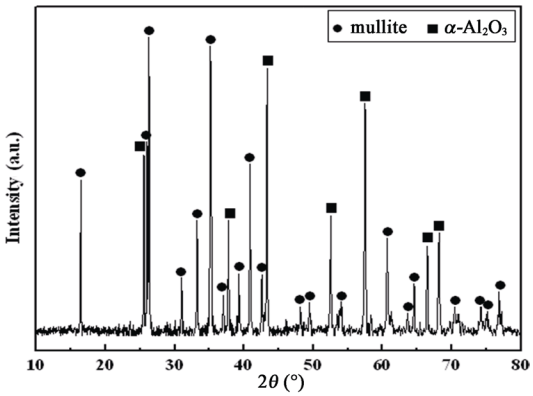

Fig. 5 XRD patterns of Al_2O_3–SiO_2 gel powders after heat treatment at 1600 ℃.

two-thirds and a weight loss of 17.2% was observed. At the same time, carbon fiber was chemically damaged to a great extent, leading to sharp degradation in flexural strength and fracture work.

As shown in Fig. 6, the fiber pull-out and interfacial debonding were still obvious after annealing at 1200 ℃, corresponding to the unchanged mechanical properties. However, this phenomenon was obscure at 1400 ℃ due to the activated interfacial reaction. After annealing at 1600 ℃, the flat fracture surface was formed. Moreover, the cross-section shape of carbon fiber was distorted and the interspace between fiber and matrix was clear. These could be attributed to the above-mentioned severe carbothermal reduction.

In order to protect carbon fiber from chemical damage, PyC coating was prepared on the surface of carbon fiber by CVD. The resulting composites were called C/PyC/mullite composites. SEM appearances of the PyC coating are presented in Fig. 7. As shown, carbon fiber was well coated and the coating was dense with a thickness of 0.53 μm. By adding PyC coating, the flexural strength of C/mullite composites was increased by 25.8%, reaching 288.0 MPa. The stress–strain curve and fracture surface of C/PyC/mullite composites are presented in Figs. 3 and 8, respectively. The fracture work of C/PyC/mullite composites was calculated from Fig. 3 to be 6300 J/m^2 which is a little higher than that of C/mullite composites. In Figs. 4 and 8(a), both the composites showed extensive fiber pull-out. Consequently, it is indicated that the addition of PyC interfacial coating can improve the mechanical properties of C/mullite composites. However, it seems that the positive effect of PyC coating on the mechanical properties of C/mullite composites was not very remarkable.

In addition, the differences in fracture behaviors of C/mullite and C/PyC/mullite composites are noticed in Fig. 3. As compared with C/mullite composites, C/PyC/mullite composites had higher flexural modulus and lower flexural strain (~0.6%) at invalidation point. For CVD derived PyC coating, it was dense and bonded to carbon fiber tightly, thus enhancing the physical bonding of interface. The enhanced interfacial bonding can effectively transfer the load from matrix to carbon fiber. For continuous fiber reinforced ceramic matrix composites, fiber is the main load bearer. Accordingly, the flexural strength and modulus were improved. At the same time, the enhanced interfacial bonding is disadvantageous to the dissipation of crack-tip energy, leading to the decrease of the invalidation strain. The thickness of PyC coating in this study was not optimal. Subsequent studies will optimize the thickness of PyC coating, then the further improvement in mechanical properties can be anticipated.

The weight loss and mechanical properties of C/PyC/mullite composites after annealing are listed in Table 3. It is clear that the C/PyC/mullite composites

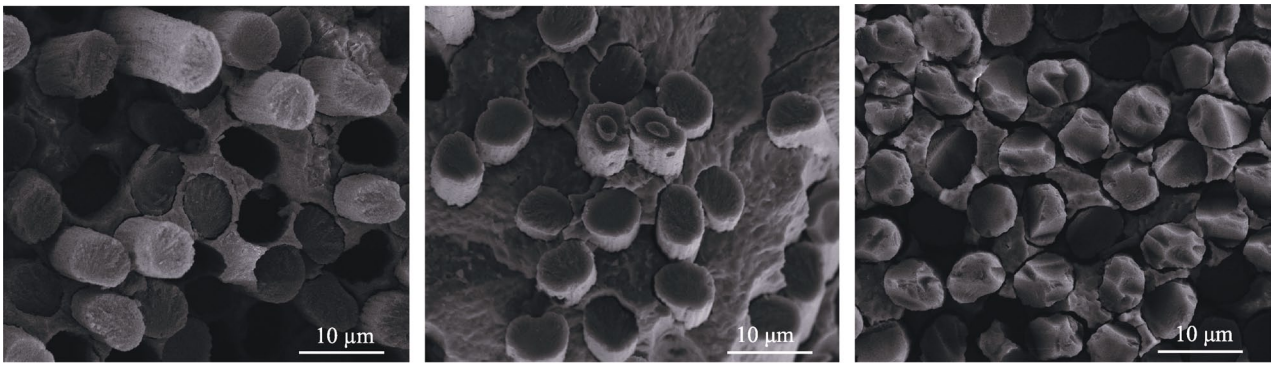

Fig. 6 Fracture surfaces of the C/mullite composites without interfacial coating after annealing at (a) 1200, (b) 1400, and (c) 1600 ℃.

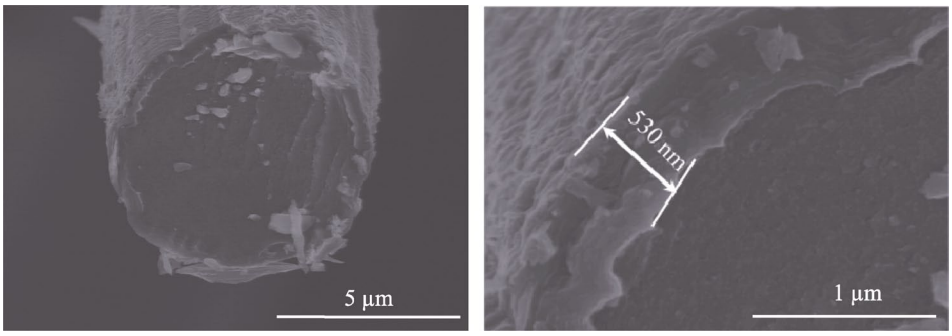

Fig. 7 SEM photos of PyC coating.

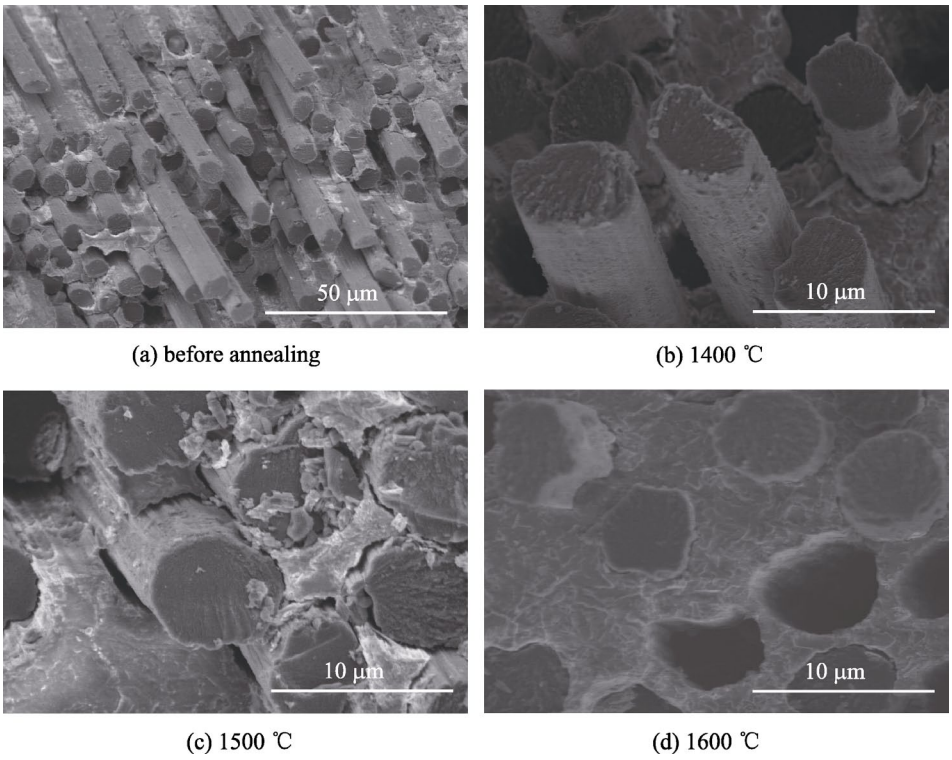

Fig. 8 Fracture surfaces of the C/PyC/mullite composites (a) before annealing and after annealing at (b) 1400, (c) 1500, and (d) 1600 ℃.

kept mechanical properties stable up to 1500 ℃. As compared with C/mullite composites, the flexural strength was retained much better for C/PyC/mullite composites after annealing at 1400 ℃ although the retention ratios of fracture work were almost equal for both composites. Even if annealing at 1600 ℃, the C/PyC/mullite composites still showed much higher retention ratios of mechanical properties.

In Fig. 8, it is found that the fracture surface of C/PyC/mullite composites after annealing at 1400 ℃ was almost the same as that of C/mullite composites. At 1500 ℃, fiber pull-out and interfacial debonding were still clear. After annealing at 1600 ℃, the pulled-out fibers lessened and the fracture surface became flat. However, the distortion of fiber and the interspace between fiber and matrix in Fig. 6 were not observed. This means that the chemical erosion of carbon fiber was effectively alleviated by the PyC coating. Therefore, it is indicated that the PyC coating can remarkably improve the thermal stability of C/mullite composites.

Table 3 Weight loss and mechanical properties of C/PyC/mullite composites after annealing

Annealing temperature (℃)	1400	1500	1600
Weight loss (%)	0.83	0.88	15.80
Strength retention ratio (%)	101.70	109.00	77.70
Fracture work retention ratio (%)	93.30	94.30	34.90

However, it is noticed that the PyC coating had little influence on the weight loss during annealing. The weight loss at 1400 ℃ was the same for both composites. After annealing at 1600 ℃, the C/PyC/ mullite composites showed a weight loss (15.80%) that was a little lower than that (17.20%) of C/mullite composites. As mentioned above, the only possible reaction between PyC and matrix was also the carbothermal reduction of $C+SiO_2$. As far as the chemical-vapor-deposited PyC was concerned, its purity and crystallinity were higher than those of the disordered carbon on fiber surface. Accordingly, the reactivity of $PyC+SiO_2$ was relatively low. As a result, the weight loss after annealing of C/PyC/mullite composites was lower.

Figure 9 shows the cross-sections of C/PyC/mullite composites before and after annealing. From room temperature to 1500 ℃, the cross-sections were very dense and the PyC coating was distinct. After annealing at 1600 ℃, it is found that some PyC coatings disappeared, creating a relatively loose cross-section. Thus, it is deemed that some PyC coatings were consumed by carbothermal reduction during annealing. It was the sacrifice of PyC coating that protected carbon fibers from chemical damage, resulting in the much higher retention ratios of mechanical properties. At the same time, the load-transfer capacity was weakened due to the disappearance of PyC coating. As a result, the absolute strength of the C/PyC/mullite composites after annealing at 1600 ℃ was not as high as original strength.

4 Conclusions

By using the laminated and stitched carbon fiber cloth preform as reinforcement and the Al_2O_3–SiO_2 sol with Al_2O_3/SiO_2 molar ratio of 3/2 as raw materials, respectively, C/mullite composites have been fabricated through the SIDH route. Owing to the characteristic of sol and the structure of preform, the total porosity and the close porosity of C/mullite composites were remarkably reduced compared with previous studies. Accordingly, the flexural strength was equivalent to that of dense mullite. The fracture toughness was notably improved due to the introduction of carbon fiber reinforcement.

The composites without interfacial coating could retain its strength up to 1200 ℃. The carbothermal reduction between carbon fiber and residual SiO_2 in matrix became active above 1200 ℃, resulting in obvious strength degradation after annealing at 1400 and 1600 ℃. By introducing PyC coating on carbon fibers, the carbothermal reduction of carbon fiber was

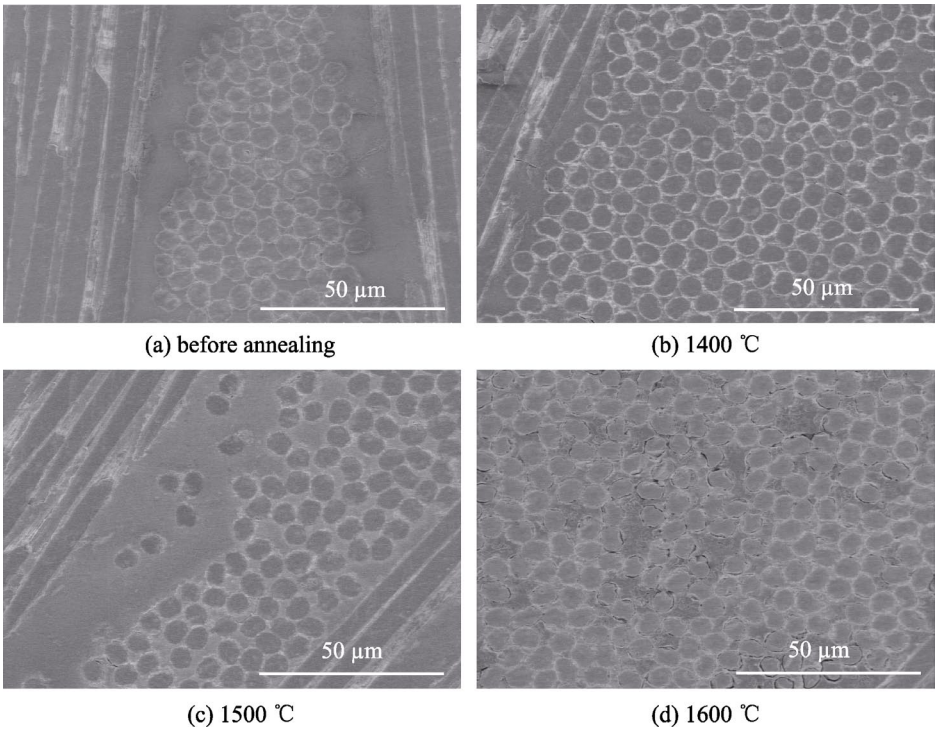

Fig. 9 Cross-section photos of the C/PyC/mullite composites (a) before annealing and after annealing at (b) 1400, (c) 1500, and (d) 1600 ℃.

effectively suppressed at the cost of the sacrifice of PyC coating, and the thermal stability of C/mullite composites was enhanced notably. For C/PyC/mullite composites, no strength degradation was detected up to 1500 ℃, and the strength retention ratio after annealing at 1600 ℃ (77.7%) was much higher than that (29.3%) of C/mullite composites.

Acknowledgements

This work was supported by the Open Foundation of Science and Technology on Thermostructural Composite Materials Laboratory (Grant No. 614291102010117), the Science Innovation Foundation of Shanghai Academy of Spaceflight Technology (Grant No. SAST2015043), and the National Natural Science Foundation of China (Grant No. 11572277).

References

[1] Schneider H, Schreuer J, Hildmann B. Structure and properties of mullite−A review. *J Eur Ceram Soc* 2008, **28**: 329–344.

[2] Abdulhameed MA, Othman MHD, Joda HNAA, *et al*. Fabrication and characterization of affordable hydrophobic ceramic hollow fibre membrane for contacting processes. *J Adv Ceram* 2017, **6**: 330–340.

[3] Kumar P, Nath M, Ghosh A, *et al*. Thermo-mechanical properties of mullite–zirconia composites derived from reaction sintering of zircon and sillimanite beach sand: Effect of CaO. *Trans Nonferrous Met Soc China* 2016, **26**: 2397−2403.

[4] Xu XH, Lao XB, Wu JF, *et al*. Effect of MnO_2 on properties of SiC-mullite composite ceramics for solar sensible thermal storage. *J Wuhan Univ Technol-Mater Sci* 2016, **31**: 491−495.

[5] Zhang JY, Zhan H, Fu ZY, *et al*. *In-situ* synthesis and sintering of mullite glass composites by SPS. *J Adv Ceram* 2014, **3**: 165–170.

[6] Ma QS, Cai LH. Fabrication and oxidation resistance of mullite/yttrium silicate multilayer coatings on C/SiC composites. *J Adv Ceram* 2017, **6**: 360–367.

[7] Wang Y, Liu HT, Cheng HF, *et al*. Effective fugitive carbon coatings for the strength improvement of 3D Nextel™ 440/aluminosilicate composites. *Mater Lett* 2014, **126**: 236−239.

[8] Wang Y, Cheng HF, Wang J. Effects of the single layer CVD SiC interphases on mechanical properties of mullite fiber-reinforced mullite matrix composites fabricated via a sol-gel process. *Ceram Int* 2014, **40**: 4707–4715.

[9] Wang Y, Cheng HF, Liu HT, *et al*. Effects of sintering temperature on mechanical properties of 3D mullite fiber (ALF FB_3) reinforced mullite composites. *Ceram Int* 2013, **39**: 9229–9235.

[10] Kaya C, Butler EG, Selcuk A, *et al*. Mullite (Nextel™ 720) fibre-reinforced mullite matrix composites exhibiting favourable thermomechanical properties. *J Eur Ceram Soc* 2002, **22**: 2333–2342.

[11] Ruggles-Wrenn MB, Kutsal T. Effects of steam environment on creep behavior of Nextel™720/alumina−mullite ceramic composite at elevated temperature. *Compos A−Appl Sc i Manuf* 2010, **41**: 1807−1816.

[12] Zok FW. Developments in oxide fiber composites. *J Am Ceram Soc* 2006, **89**: 3309–3324.

[13] Wang Y, Liu HT, Cheng HF, *et al*. Research progress on oxide/oxide ceramic matrix composites. *J Inorg Mater* 2014, **29**: 673−680. (in Chinese)

[14] Wu J, Jones FR, James PF. Continuous fibre reinforced mullite matrix composites by sol-gel processing: Part I Fabrication and microstructures. *J Mater Sci* 1997, **32**: 3361−3368.

[15] Wu J, Jones FR, James PF. Continuous fibre reinforced mullite matrix composites by sol-gel processing: Part II Properties and fracture behavior. *J Mater Sci* 1997, **32**: 3629−3635.

[16] Dong RL, Hirata Y, Sueyoshi H, *et al*. Polymer impregnation and pyrolysis (PIP) method for the preparation of laminated woven fabric/mullite matrix composites with pseudoductility. *J Eur Ceram Soc* 2004, **24**: 53–64.

[17] Xiang Y, Wang Q, Cao F, *et al*. Sol-gel process and high-temperature property of SiO_2/ZrO_2-SiO_2 composites. *Ceram Int* 2017, **43**: 854–859.

[18] Wang Q, Cao F, Xiang Y, *et al*. Effects of ZrO_2 coating on the strength improvement of 2.5D SiC_f/SiO_2 composites. *Ceram Int* 2017, **43**: 884–889.

[19] Fan CY, Ma QS, Zeng KH. Thermal stability and oxidation resistance of C/Al_2O_3 composites fabricated from a sol with high solid content. *Ceram Int* 2017, **43**: 10983–10990.

[20] Shan BR, Ma QS, Zeng KH. Fabrication of three-dimensional carbon fiber preform reinforced YAG composites from a sol with high solid content. *Ceram Int* 2018, **44**: 4478–4482.

[21] Shan BR, Ma QS, Zeng KH. Microstructure and mechanical properties of carbon fiber needled felt reinforced sol-derived YAG composite. *J Alloys Compd* 2019, **772**: 381–387.

[22] Liu HT, Ma QS, Liu WD. Mechanical and oxidation resistance properties of 3D carbon fiber-reinforced mullite matrix composites prepared by sol-gel process. *Ceram Int* 2014, **40**: 7203–7212.

[23] Liang SL, Ma QS, Liu HT, *et al*. Fabrication and mechanical properties of three-dimensional carbon fiber reinforced (Al_2O_3-SiO_2) matrix composites. *Rare Metal Mater Eng* 2016, **45**: 585−589. (in Chinese)

[24] Zhang W, Ma QS, Dai KW, *et al*. Preparation of three-dimensional braided carbon fiber reinforced mullite composites from a sol with high solid content. *Trans Nonferrous Met Soc China* 2018, **28**: 2248–2254.

[25] Zhang W, Ma QS, Dai KW, *et al*. Fabrication and properties

of three-dimensional braided carbon fiber reinforced SiO_2-rich mullite composites. *J Wuhan Univ Technol–Mater Sci* (accepted).

[26] Yan M, Song W, Chen ZH. *In situ* growth of a carbon interphase between carbon fibres and a polycarbosilane-derived silicon carbide matrix. *Carbon* 2011, **49**: 2869–2872.

[27] Liu HT, Yang LW, Sun X, *et al*. Enhancing the fracture resistance of carbon fiber reinforced SiC matrix composites by interface modification through a simple fiber heat-treatment process. *Carbon* 2016, **109**: 435–443.

[28] Liu YS, Cheng LF, Zhang LT, *et al*. Fracture behavior and mechanism of 2D C/SiC-BC_x composite at room temperature. *Mater Sci Eng* 2011, **528**: 1436–1441.

[29] Cividanes LS, Campos TMB, Rodrigues LA, *et al*. Review of mullite synthesis routes by sol–gel method. *J Sol-Gel Sci Technol* 2010, **55**: 111–125.

[30] Wu J, Chen M, Jones FR, *et al*. Characterisation of sol-gel derived alumina-silica matrices for continuous fibre reinforced composites. *J Eur Ceram Soc* 1996, **16**: 619–626.

[31] Treadwell DR, Dabbs DM, Aksay IA. Mullite ($3Al_2O_3$–$2SiO_2$) synthesis with aluminosiloxanes. *Chem Mater* 1996, **8**: 2056–2060.

[32] Tkalcec E, Ivankovic H, Nass R, *et al*. Crystallization kinetics of mullite formation in diphasic gels containing different alumina components. *J Eur Ceram Soc* 2003, **23**: 1465–1475.

[33] Vix-Guterl C, Ehrburger P. Effect of the properties of a carbon substrate on its reaction with silica for silicon carbide formation. *Carbon* 1997, **35**: 1587–1592.

[34] Yang T, Chen JH, Li LD, *et al*. Template free synthesis of highly ordered mullite nanowhiskers with exceptional photoluminescence. *Ceram Int* 2015, **41**: 9560–9566.